

Supplemental Information for

Photocatalytic syngas production from bio-derived glycerol and water on AuIn-decorated GaN nanowires supported by Si wafer

Zhouzhou Wang^{1,2+}, Bowen Sheng³⁺, Yiqing Chen⁴⁺, Sharif Md. Sadaf⁵, Jinglin Li¹, Jiajia Yang³, Jun Song^{4*}, Lin Yao⁶, YingYu^{2*}, Lei Zhu¹, Xinqiang Wang^{3,7,8*}, Zhen Huang¹, Baowen Zhou^{1*}.

1. Key Laboratory for Power Machinery and Engineering of Ministry of Education, School of Mechanical Engineering, Shanghai Jiao Tong University, 800 Dongchuan Road, Shanghai 200240, China.
2. Institute of Nanoscience and Nanotechnology, College of Physical Science and Technology, Central China Normal University, Wuhan 430079, China.
3. State Key Laboratory of Artificial Microstructure and Mesoscopic Physics, School of Physics, Nano-Optoelectronics Frontier Center of Ministry of Education (NFC-MOE), Peking University, Beijing 10087, China.
4. Department of Mining and Materials Engineering, McGill University, 3610 University Street, Montreal, QC H3A0C9, Canada.
5. Centre Energie, Matériaux et Télécommunications, Institut National de la Recherche Scientifique (INRS)-Université du Québec, 1650 Boulevard Lionel-Boulet, Varennes, Quebec J3X1S2, Canada
6. China-UK Low Carbon College, Shanghai Jiao Tong University, 3 Yinlian Road, Shanghai 201306, China.
7. Peking University Yangtze Delta Institute of Optoelectronics, Nantong, Jiangsu 226010, China
8. Collaborative Innovation Center of Quantum Matter, School of Physics, Peking University, Beijing 100871, China.

* Corresponding authors Email: jun.song2@mcgill.ca; yuying01@mail.ccnu.edu.cn; wangshi@pku.edu.cn; zhoubw@sjtu.edu.cn.

+ These authors contributed equally to this work.

Experimental section

Material synthesis

Materials. The chemicals were directly used without purification offered by commercial companies. Glycerol was purchased from RHAWN Reagent (99%, AR grade).

The fabrication of 1D GaN NWs/Si wafer hybrid architecture. Catalyst-free GaN NWs were grown on a 4-inch Si (111) wafer substrate by a radio-frequency plasma-assisted SVTA MBE system under nitrogen-rich conditions. All the nanowires are of N-face polarity. First, the standard pre-growth processes including high temperature degas and nitridation were performed as the former report ¹. The nanowire growth was carried out maintaining constant nitrogen flux and growth temperature of $\sim 700^\circ\text{C}$. The growth temperatures were measured by a calibrated pyrometer. The nanowire consists of approximately 400 nm unintentionally doped GaN and 500 nm p-GaN (Mg-doped) layer. At first, undoped GaN NW bases with a height of about 400 nm were grown. Subsequently, the Mg-doped GaN upper parts were grown in multiple-steps by switching Mg cell temperatures in the order of 230°C , 250°C and 270°C (Mg and/or hole concentrations were intentionally varied by changing Mg flux and/or cell temperature). To be noted, the GaN nanowires have been grown using a continuous growth process without any growth interruption by changing only Mg flux. It is worthwhile mentioning that it is difficult to precisely know the hole density at different Mg flux as there is no known and reliable technique to measure Mg and/or density in nanowires. It is expected that the nanowire architecture can be further optimized to get selective and efficient syngas.

The coupling of dual gold-indium cocatalyst with GaN NWs on Si wafer. The deposition of AuIn NPs on GaN NWs was carried out using a simple one-step photo-deposition process. Firstly, the GaN NWs sample was placed into a 0.4 L quartz chamber poured into 40 ml of 10 wt.% glycerol solution, followed by the addition of different volume of chloroauric acid aqueous solution (H_2AuCl_4 , 0.2 M) and indium chloride (InCl_3 , 0.2 M). Then, the chamber was irradiated using a 300 W xenon lamp (AuLight, CEL-HLF300-T3) for 30 min under argon (Ar) atmosphere. Finally, the assembled AuIn NPs/GaN NWs/Si was rinsed with distilled water thoroughly. For comparison, AuIn/Si and AuIn/GaN/Sapphire were fabricated by employing various

semiconductor platforms using identical process.

Materials characterizations

The X-ray diffraction (XRD) profile data were collected by a Bruker D8 Advance diffractometer (with Cu K α , at 60 kV and 80 mA) in continuous scanning mode over a 2 θ range of 20-80 degrees. The X-ray photoelectron spectroscopy (XPS) was collected by an ESCALAB 250xi non-monochromatic Al anodes, and the binding energy of C1s at 284.8 eV was used for the internal calibration. The loading density of catalyst was evaluated by an inductively coupled plasma-atomic emission spectroscopy (AGILENT ICP-OES 730). High-angle annular dark field-scanning transmission electron microscopy (HAADF-STEM) and energy dispersive X-ray spectroscopy (EDS) were performed using a Thermo Fisher Scientific Talos F200X S/TEM, equipped with a Super-X EDS detector and operated at 200 kV. Scanning electron microscopy (SEM) images were conducted using a Quattro ESEM (Thermo Fisher). Transmission electron microscopy (TEM) images were conducted using a JEOL 2100F microscope at 200 kV. The electron paramagnetic resonance (EPR) measurements were performed on a Bruker A300 spectrometer under room temperature using TEMPO as the trapping agent. Photoluminescence (PL) characterization was performed using a 325 nm wavelength with pulsed laser with excitation frequency of 80 MHz by the third harmonic generation of a Ti: Sapphire laser. The beam was focused from a steep angle to a ~ 6 μm spot on the sample collected using a 40 \times magnification microscope objective with the numerical aperture of 0.65 and then directed to a cooled charge coupled device (CCD) spectrometer using an 1800 mm^{-1} reflection grating. The diffuse reflectance UV-Vis-IR spectroscopy characterization was conducted using a Thermo Scientific Evolution 600 UV-Vis-NIR spectroscope. The gas chromatography mass spectrum (GC-MS) was carried out for the detection of liquid productions using a TRACE 1300, ISQ 7000, Thermo Scientific.

Photocatalytic reactions

Unless specifically noted, the reactions were performed in a 0.39 L home-made sealed quartz chamber² under illumination by a 300 W Xenon lamp (AuLight, CEL-HLF300-T3) without stirring and temperature controlling. Typically, the as-designed AuIn/GaN was placed at the

bottom of the chamber. 1 ml of glycerol solution with desired concentration was then transferred into the chamber. The system was then well evacuated and filled with argon (Ar), followed by irradiated with the light intensity of 4 W/cm². The gaseous products were extracted by a sealed syringe without using a purge gas and transferred into a gas chromatograph (GC-9080, Sun) equipped with a flame ionization detector (FID) and thermal conductivity detector (TCD) for analysis ². Each experiment is carried out three times, and the average is taken as its actual value. The hydroxyl radical trapping experiment using TEMPO was carried out under the irradiation intensity of 2.5 W/cm².

Calculation of reaction performance activity of H₂, CO

$$n = \frac{V_{chamber} \times n_1}{V_m}$$

$$Gas\ Yield\ Rate = \frac{n}{S \times W \times T}$$

$$TOF = \frac{n}{S \times T \times Loading\ Density}$$

where $V_{chamber}$ is the total gas volume of the reaction chamber, 0.3 L. V_m is the gas molar volume under standard conditions, 22.4 L/mol. n_1 is the target gas concentration measured by GC. n is the produced molar amount of target gas. S is the geometric surface of the sample. W is the total weight of the epitaxial of GaN NWs, estimated to be ~0.1 mg/cm², without considering the weight of trace AuIn cocatalyst. T is the reaction time. *Loading Density* of AuIn cocatalyst is evaluated to be ~0.05 μmol/cm² by ICP-AES. *TOF* is the turnover frequency.

Theoretical calculations

Computational methods. Spin-polarized density functional theory (DFT) calculations ³ were performed employing the Vienna Ab Initio Simulation Package (VASP) ^{4,5}. The interactions of electrons with ion cores were represent by the projector-augmented wave (PAW) method ⁶, and the exchange-correlation was described by the Perdew-Burke-Ernzerhof (PBE) functional ^{7,8}. A

kinetic cutoff energy of 500 eV was set for the plane-wave basis functions. The Brillouin zone was sampled by a $2 \times 2 \times 1$ k-point grid. Grimme's DFT-D3 method with Becke-Johnson damping was applied to include the effect of weak van der Waals (vdW) interactions^{9,10}.

Model construction. A 6×6 GaN slab with 6 layers and surface orientation of $[10\bar{1}0]$ was constructed based on the experimental results, denoted as the GaN($10\bar{1}0$) model. Based on the GaN($10\bar{1}0$) model, the models of In₄/GaN and In₃Au/GaN were constructed by depositing a small metal cluster on the GaN slab, and their lowest-energy configurations were identified by DFT calculations and selected as the models used in the calculations. In addition to the above models with a GaN substrate, we constructed Au/In interface model consisting of an Au cluster deposited on the most energetically stable surface of In, i.e., In(101). This model is denoted as Au₄/In(101) and was used to investigate the effect of the Au/In interface on glycerol adsorption. All atoms except those in the bottom three layers of the GaN slab and in the bottom layer of Au₄/In(101) were relaxed until the residual forces were smaller than 0.03 eV/Å and the electronic energy converged to 10⁻⁴ eV. To avoid periodic image interactions, a vacuum layer of at least 15 Å was set along the direction perpendicular to the substrate slab (i.e., GaN or In(101)) for all models.

Gibbs free energy and adsorption site. The Gibbs free energy of adsorption ΔG was calculated as:

$$\Delta G = E_{ad} + \Delta ZPE + \int \Delta C_p dT - T\Delta S \quad (1)$$

where the adsorption energy (E_{ad}) of an adsorbate on the modelled catalyst surface is defined as:

$$E_{ad} = E_{adsorbate/surface} - E_{adsorbate} - E_{surface} \quad (2)$$

where $E_{adsorbate/surface}$, $E_{adsorbate}$ and $E_{surface}$ are the total energies of the adsorption configuration, adsorbate in the gas phase, and the clean surface. ΔZPE is the change in zero-point energy, ΔC_p is the heat capacity and ΔS represents the entropy of a species. The temperature T is set to 298.15 K.

Adsorption of glycerol on surfaces of the models constructed, i.e., GaN($10\bar{1}0$), In₄/GaN, In₃Au/GaN, and Au₄/In(101) (See **Fig. 1** and **Fig. S3**), were then investigated. It is found that O

atoms from glycerol bind strongly with the Ga atoms underneath for the case of GaN($10\bar{1}0$), In₄/GaN and In₃Au/GaN, with negative ΔG_{ad} values of -0.34, -1.45 and -1.39 eV, respectively. In contrast, glycerol floats above Au₄/In(101) surface with ΔG_{ad} values around 0 eV, indicative of negligible interaction of glycerol with this surface. The above observations illustrate the importance of the presence of GaN in the catalytic system. These findings also confirm that the adsorption site of glycerol is at the GaN surface. All processes are considered under solvent effects

11.

Supplementary Figures

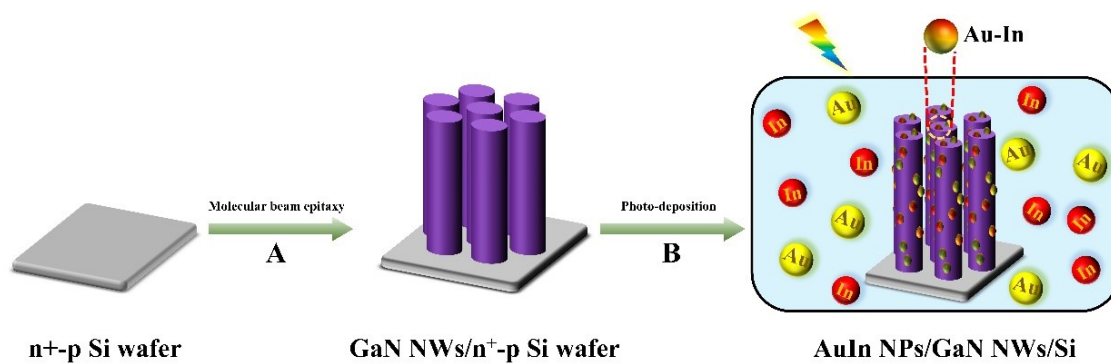


Fig. S1 Schematic assembly of AuIn NPs/GaN NWs/Si by combining molecular beam epitaxy synthesis with photo-deposition.

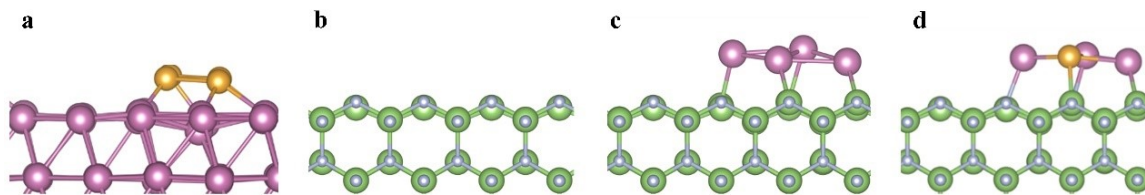


Fig. S2 Side views of optimized configurations of (a) Au/In, (b) GaN, (c) In₄/GaN and (d) In₃Au/GaN. Ga, green; N, silver; In, purple; and Au, gold.

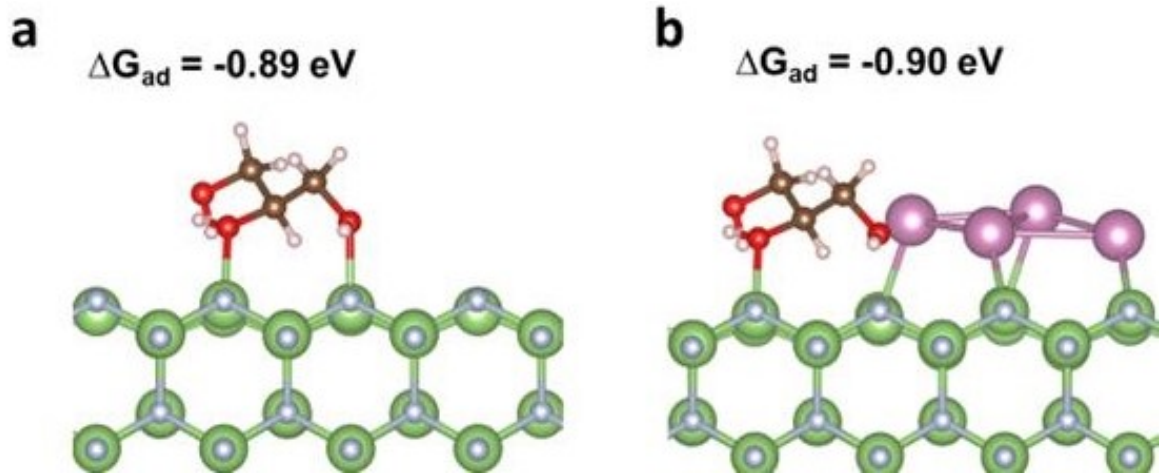


Fig. S3 Side views of optimized glycerol adsorption configurations of (a) GaN, (b) In₄/GaN. Ga, green; N, silver; In, purple; C, brown; H, pink; and O, red.

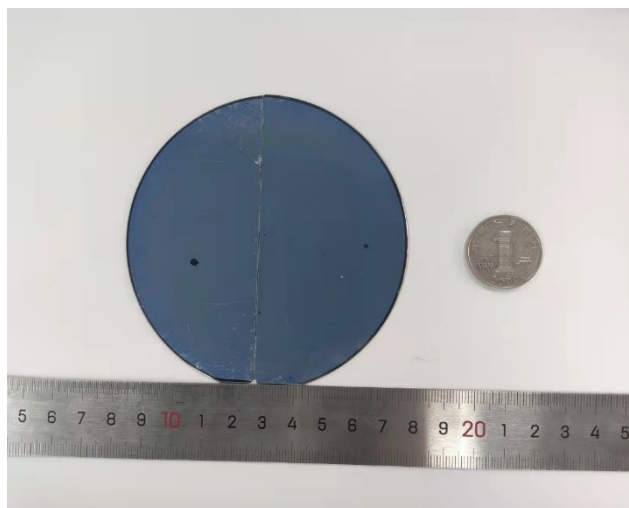


Fig. S4 The digital photo of GaN NWs/Si wafer.

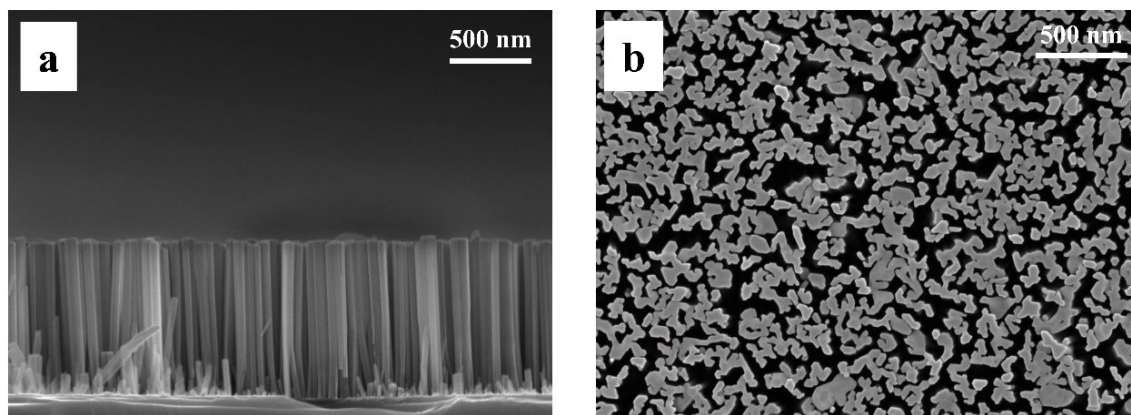


Fig. S5 (a) Front and (b) top views of GaN NWs/Si wafer.

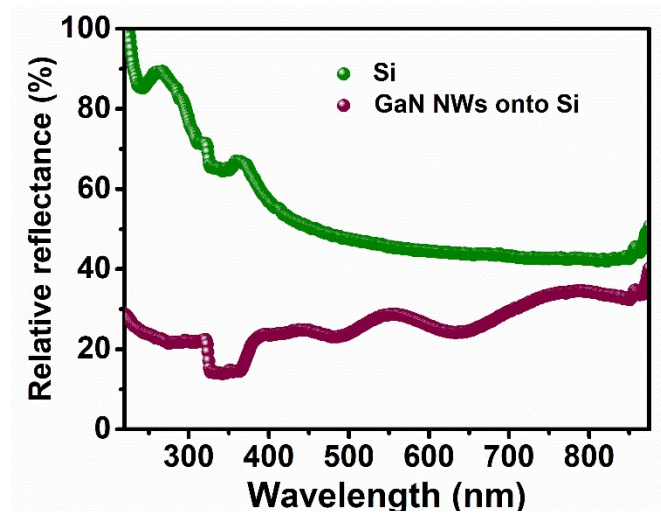


Fig. S6 Diffuse reflectance ultraviolet-visible-near infrared light spectroscopy of Si wafer and GaN NWs vertically aligned onto Si wafer.

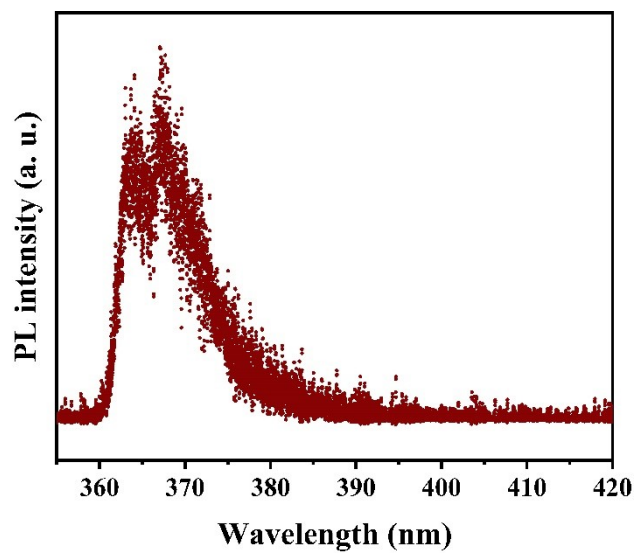


Fig. S7 Photoluminescence spectra of GaN NWs onto Si wafer.

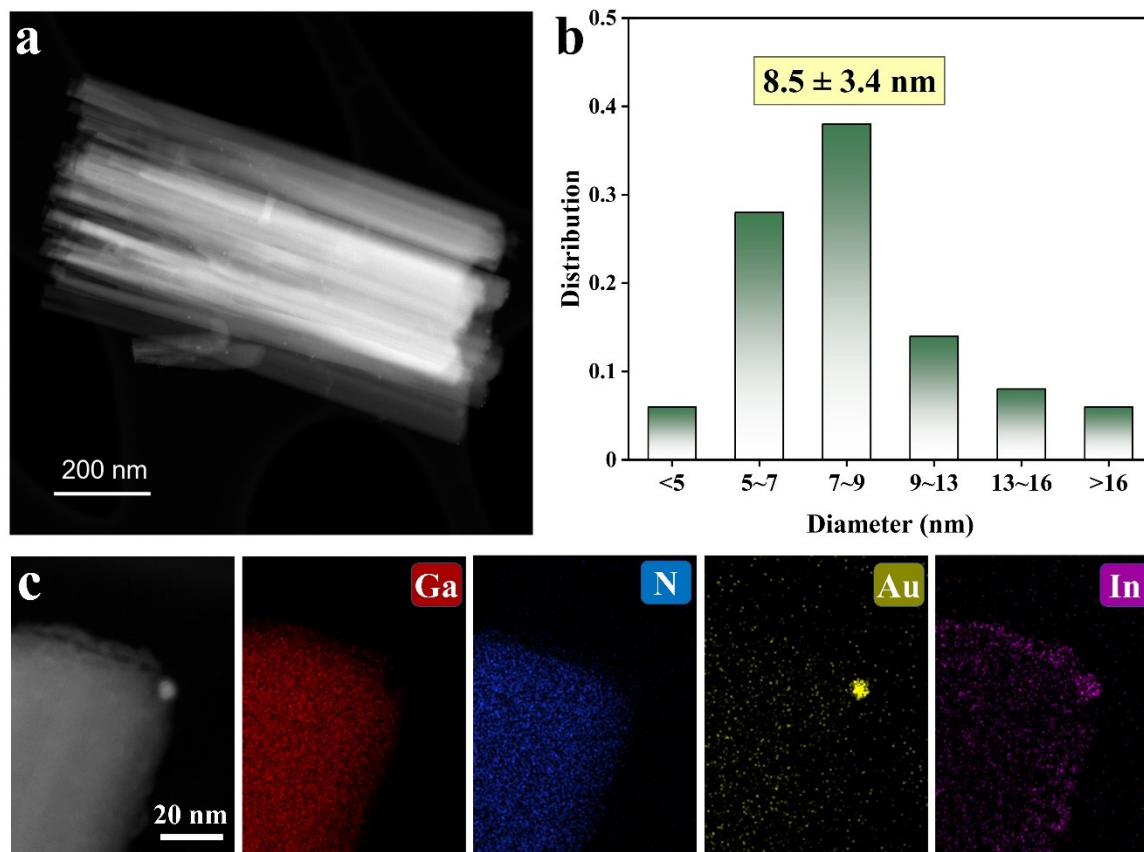


Fig. S8 (a) HAADF-STEM image of AuIn NPs/GaN NWs and (b) the size distribution of AuIn NPs. (c) HAADF-STEM image and the elemental mapping images.

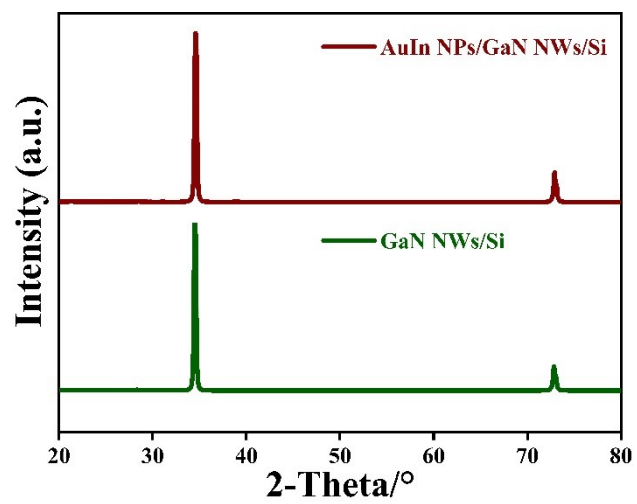


Fig. S9 XRD spectrum of AuIn NPs/GaN NWs/Si and GaN NWs/Si.

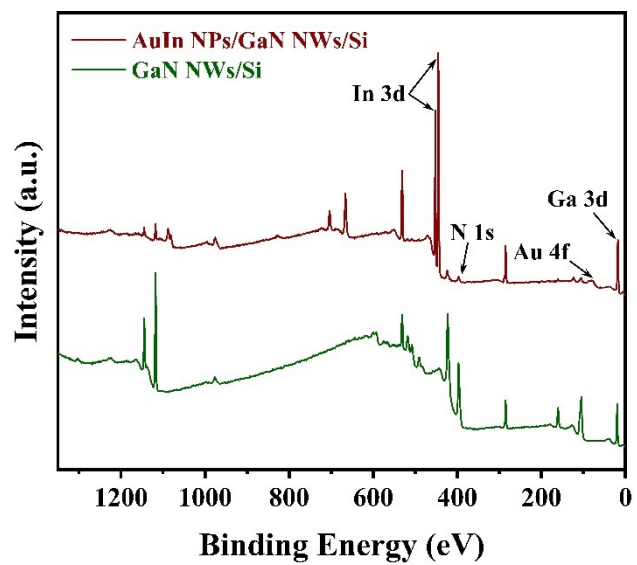


Fig. S10 XPS survey spectrum of AuIn NPs/GaN NWs/Si and GaN NWs/Si.

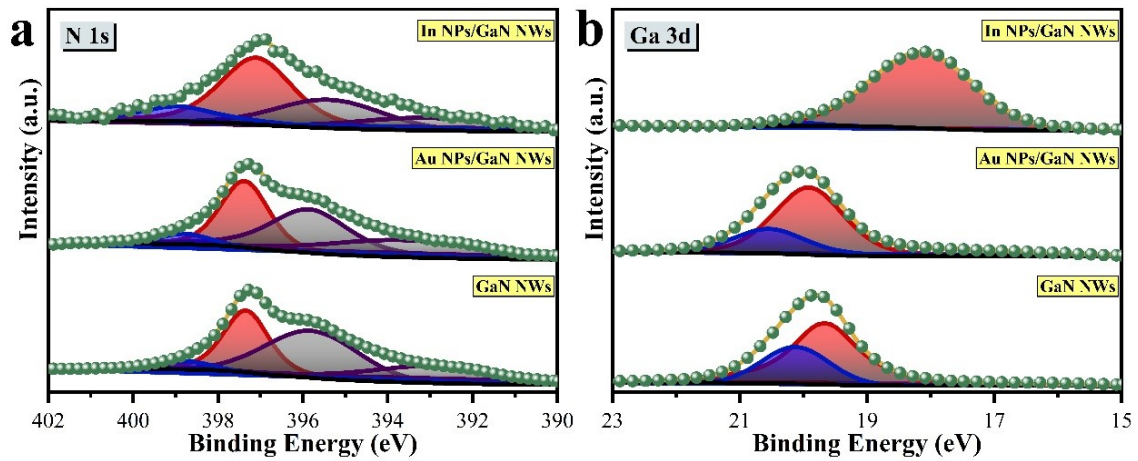


Fig. S11 XPS spectrum of (a) N1s and (b) Ga3d of In NPs/GaN NWs, Au NPs/GaN NWs, and GaN NWs.

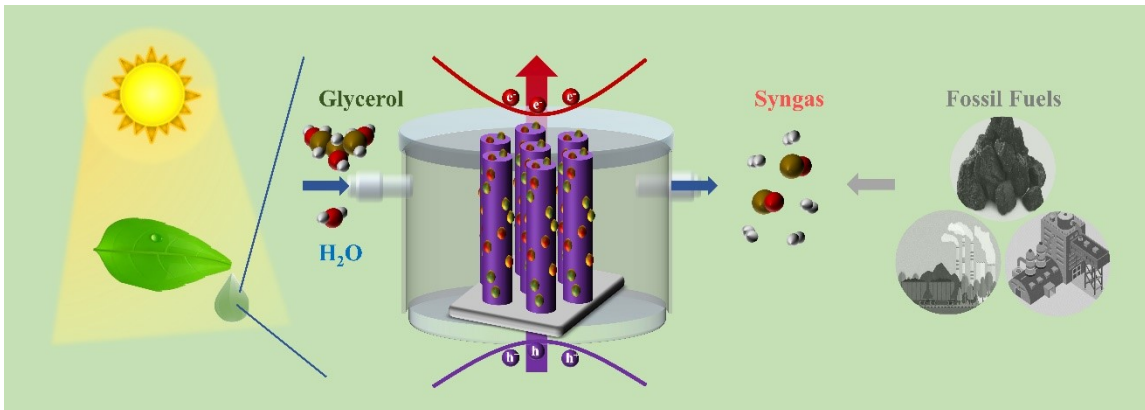


Fig. S12 Schematical illustration of light-driven conversion of glycerol and water toward syngas, which is substantially distinct from the conventional route built on fossil fuels.

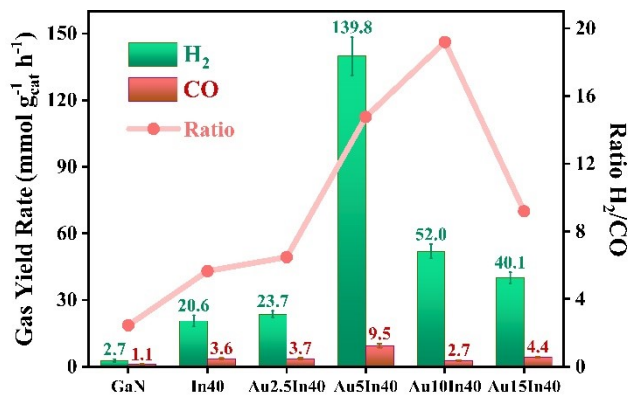


Fig. S13 Influence of the Au/In ratios with an unvaried In on the reaction. Experimental conditions: 300 W Xenon lamp, light intensity, 4 W·cm⁻², 1 ml of glycerol aqueous solution (weight ratio, 5% glycerol), atmospheric argon pressure.

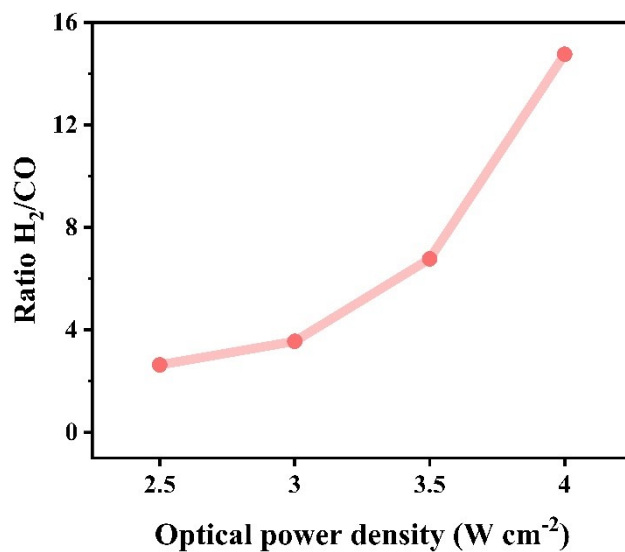


Fig. S14 Influence of the optical power density on the H₂/CO ratio of AuIn/GaN NWs onto wafer-scale Si. Experimental conditions: 300 W Xenon lamp, 1 ml of glycerol aqueous solution (weight ratio, 5% glycerol), atmospheric argon pressure.

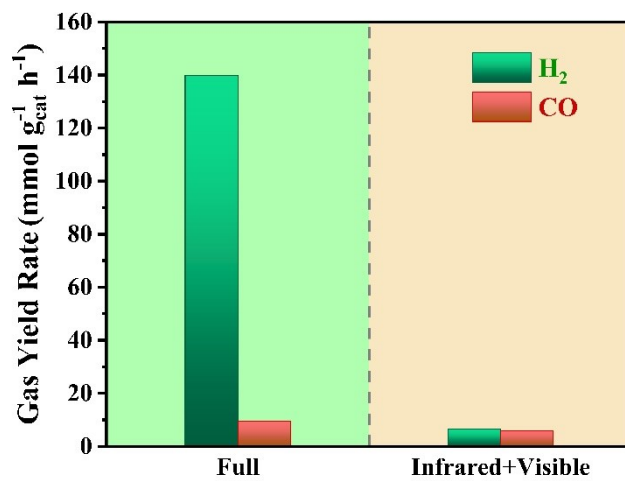


Fig. S15 Influence of the light wavelength on the syngas activity of AuIn/GaN NWs onto wafer-scale Si. Experimental conditions: 300 W Xenon lamp, 1 ml of glycerol aqueous solution (weight ratio, 5% glycerol), atmospheric argon pressure.

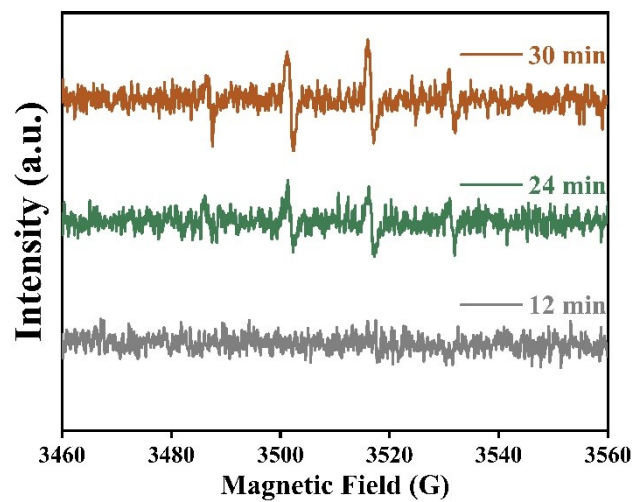


Fig. S16 In situ electron paramagnetic resonance spectroscopy measurement over AuIn/GaN NWs onto wafer-scale Si.

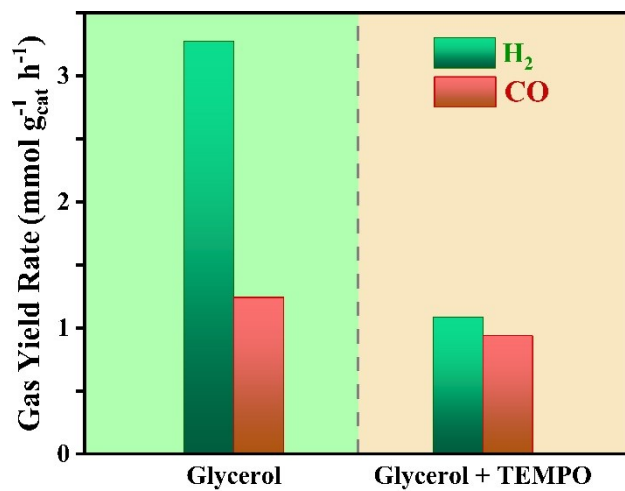


Fig. S17 Influence of the introduced TEMPO on the syngas activity of AuIn/GaN NWs onto wafer-scale Si. Experimental conditions: 300 W Xenon lamp, light intensity, 2.5 W·cm⁻², 1 ml glycerol aqueous solution (weight ratio, 5% glycerol), atmospheric argon pressure.

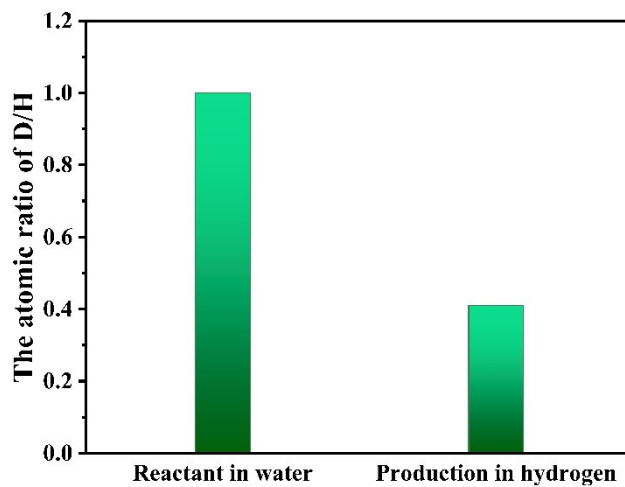


Fig. S18 The atomic ratio of D/H for the reactant in water and the production in hydrogen. Experimental conditions: 300 W Xenon lamp, light intensity, $4 \text{ W}\cdot\text{cm}^{-2}$, 1 ml glycerol aqueous solution (weight ratio, 5% glycerol), atmospheric argon pressure.

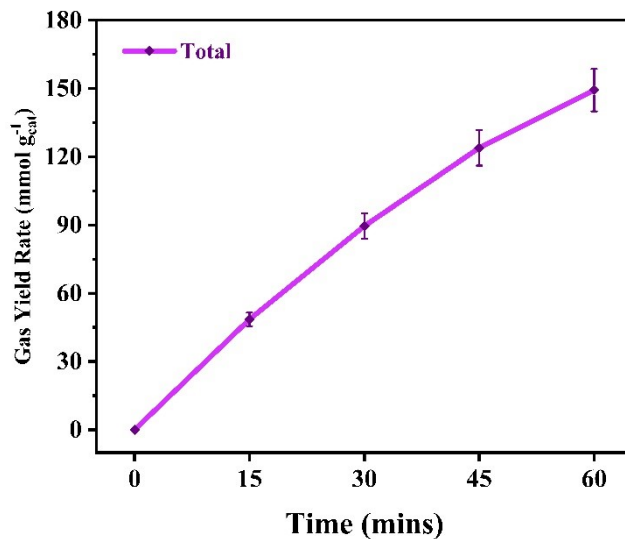


Fig. S19 The time evolution of syngas. Experimental conditions: 300 W Xenon lamp, light intensity, $4 \text{ W}\cdot\text{cm}^{-2}$, 1 ml glycerol aqueous solution (weight ratio, 5% glycerol), atmospheric argon pressure.

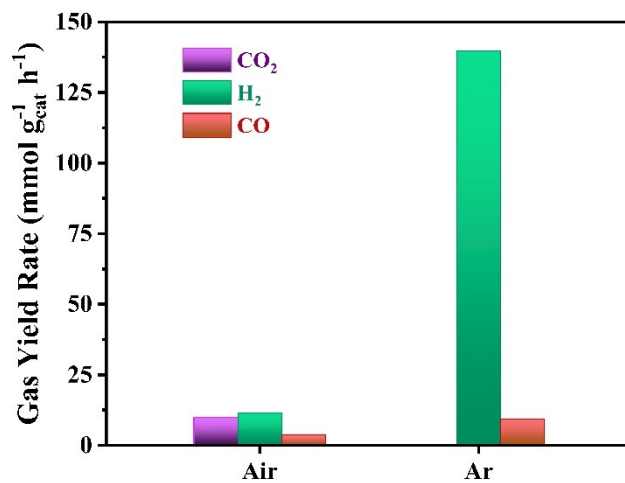


Fig. S20 The syngas and dioxide production under air or argon atmosphere. Experimental conditions: 300 W Xenon lamp, light intensity, 4 W·cm⁻², 1 ml glycerol aqueous solution (weight ratio, 5% glycerol), atmospheric air/argon pressure.

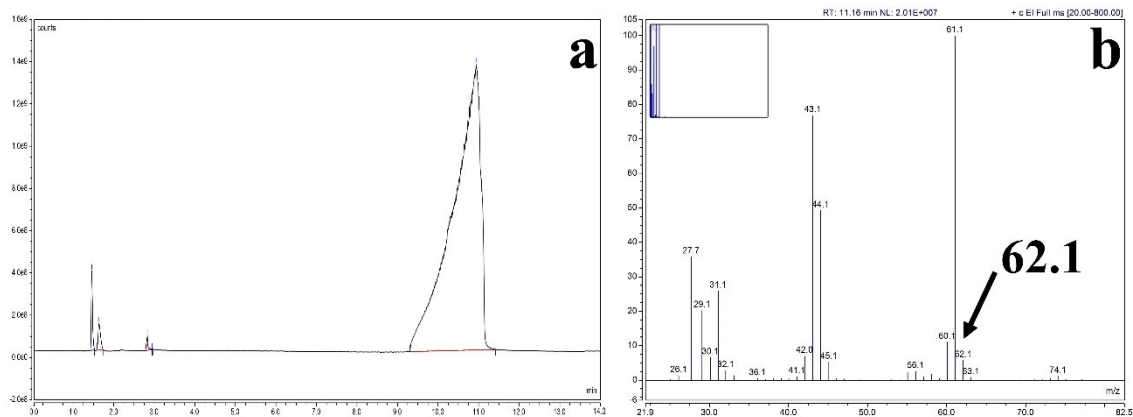


Fig. S21 (a) The result of GC test for the liquid productions and (b) the corresponding mass spectrometry at 11.16 min.

Table S1. Gibbs free energy of glycerol adsorption ΔG_{ad} on various substrates with and without solvation corrections.

Catalyst	ΔG_{ad} without solvation (eV)	ΔG_{ad} with solvation (eV)
In ₃ Au	-0.01	0.03
GaN	-0.34	-0.89
In ₄ /GaN	-1.45	-0.90
In ₃ Au/GaN	-1.39	-0.78

Table S2 ICP-OES analysis of AuIn NPs/GaN NWs/Si wafer.

Co-catalyst	Loading density of Au ($\mu\text{mol cm}^{-2}$)	Loading density of In ($\mu\text{mol cm}^{-2}$)	Total loading density ($\mu\text{mol cm}^{-2}$)
Au5	0.006	0	0.006
In40	0	0.068	0.068
Au5In40	0.005	0.048	0.053
Au10In40	0.010	0.049	0.059
Au5In80	0.005	0.120	0.125

References

1. S. Yang, H. Song, Y. Peng, L. Zhao, Y. Tong, F. Kang, M. Xu, B. Sun and X. Wang, *Nano Res.*, 2021, **14**, 3616–3620.
2. R. T. Rashid, Y. Chen, X. Liu, F. A. Chowdhury, M. Liu, J. Song, Z. Mi and B. Zhou, *Proc. Natl. Acad. Sci. U. S. A.*, 2022, **119**, e2121174119.
3. W. Kohn and L. J. Sham, *Phys. Rev.*, 1965, **140**, A1133–A1138.
4. G. Kresse and D. Joubert, *Phys. Rev. B*, 1999, **59**, 1758–1775.
5. G. Kresse and J. Furthmüller, *Phys. Rev. B*, 1996, **54**, 11169–11186.
6. P. E. Blöchl, *Phys. Rev. B*, 1994, **50**, 17953–17979.
7. J. P. Perdew, K. Burke and M. Ernzerhof, *Phys. Rev. Lett.*, 1996, **77**, 3865–3868.
8. J. P. Perdew, J. A. Chevary, S. H. Vosko, K. A. Jackson, M. R. Pederson, D. J. Singh and C. Fiolhais, *Phys. Rev. B*, 1992, **46**, 6671–6687.
9. S. Grimme, J. Antony, S. Ehrlich and H. Krieg, *J. Chem. Phys.*, 2010, **132**, 154104.
10. S. Grimme, S. Ehrlich and L. Goerigk, *J. Comput. Chem.*, 2011, **32**, 1456–1465.
11. K. Mathew, R. Sundararaman, K. Letchworth-Weaver, T. A. Arias and R. G. Hennig, *J. Chem. Phys.*, 2014, **140**, 084106.